IEEE Access
Multidisciplinary | Rapid Review | Open Access Journal

Received April 8, 2021, accepted April 15, 2021, date of publication April 20, 2021, date of current version April 29, 2021.

Digital Object Identifier 10.1109/ACCESS.2021.3074367

Hyperchaotic Self-Oscillations of Two-Stage Class C Amplifier With Generalized Transistors

JIRI PETRZELA
Department of Radio Electronics, Brno University of Technology, 616 00 Brno, Czech Republic
e-mail: petrzelj@feec.vutbr.cz

This work was supported by the Grant Agency of Czech Republic under Project GA19-22248S.

ABSTRACT This paper yields process of development, numerical analysis, lumped circuit modeling, and experimental verification of a new hyperchaotic oscillator based on the fundamental topology of two-stage amplifier. Analyzed network structure contains two generalized bipolar transistors connected with common emitter. Both transistors are initially modeled as two-ports via full admittance matrix, considering linear backward trans-conductance and polynomial forward trans-conductance. As proved in paper, these two scalar nonlinearities can push amplifier to exhibit robust hyperchaotic behavior with significantly high Kaplan-Yorke dimension. Regions of chaos and hyperchaos in a space of admittance parameters associated with both transistors are specified following the concept of positive values of Lyapunov exponents. Long time structural stability of generated hyperchaotic waveforms is proved by construction of flow-equivalent electronic circuit and experimental measurement, that is by screenshots captured by oscilloscope.

INDEX TERMS Admittance parameters, bipolar transistor, class C amplifier, chaos, chaotic oscillator, hyperchaos, Lyapunov exponents, strange attractors.

I. INTRODUCTION

Theoretical and practical investigation of chaotic behavior in the lumped electronic systems is a mature, but still up-to-date research topic. Chaotic dynamics has several properties that can be considered as somehow unique: continuous wideband frequency spectrum, sensitivity to tiny changes of the initial conditions, existence of a dense state attractor with fractional geometrical dimension, generates waveforms with increased entropy. Importantly, such kind of a complicated dynamical motion is not restricted to algebraically complex electronic systems or, more generally speaking, mathematical models. As proved in pioneering papers [1]–[5] chaotic flows can be very simple and covered by a set of the ordinary differential equations with five terms including scalar nonlinearity. These requisites are sufficient to provide necessary stretching and folding mechanism within a vector field and formation of the strange attractors. Mathematical description of deterministic non-autonomous chaotic system can be even simpler [6].

Undoubtedly, the most famous analog chaotic system is also the oldest one, and probably the most analyzed, Chua's oscillator [7]–[10]. After its discovery in 80's chaos becomes to be sought in other analog building blocks very intensively.

The associate editor coordinating the review of this manuscript and approving it for publication was Di He.

In nearly four subsequent decades, many chaotic dynamical systems were discovered; either accidentally, during investigation of mathematical model associated with a real physical phenomenon, or by using numerical algorithms dedicated for chaos localization [11], [12]. Let us discuss few cases of such chaotic dynamics within electronic systems.

For starters, paper [13] demonstrates that inductor can be removed from the Chua's oscillator and robust chaos can be generated by passive ladder network composed by resistors and capacitors. Nonlinear device is included as two-terminal piecewise-linear active resistor serving as ladder termination. Another nice example of chaotic oscillator with RC passive feedback is provided in paper [14]. Interesting cookbook [15] provides complete methodology for circuit implementation of chaotic oscillators with passive only nonlinear elements. Slight extension of these ideas leads to design of the chaotic oscillator based on second-order dynamics of supercapacitor, see paper [16] for details. Single higher-order ordinary differential equations are good prototypes for a chaos generation. Moreover, such mathematical models can be transformed to flow-equivalent circuits by looping low-pass frequency filter of arbitrary topology and active two-port having a prescribed polynomial transfer function [17]. Another design method is based on taking well-known structure of harmonic oscillator and placing single nonlinear circuit component. For

example, successful modification for Wien-bridge oscillator is shown in several papers [18]–[20]. Harmonic oscillators can be forced to evolve chaotically under specific biasing scenario, as it is theoretically and experimentally proved in paper [21], [22] for Colpitts and Hartley oscillator, respectively.

There are many methods how to construct lumped analog chaotic circuit if a describing mathematical model is known. For voltage-mode operational regime, straightforward design approach is presented in a comprehensive tutorial paper [23]. This method is known as the analog computer concept and is utilized in many papers [24]–[27]. Universality of this method is paid by serious disadvantage: complexity of final oscillator with many active devices needed. Current-mode and mixed-mode design process toward chaotic oscillators are presented, together with few examples, in review paper [28]. It is shown that final network structure can be simplified if current signal processing active elements are utilized. Of course, current mode subcircuits suitable for design of chaotic oscillators can be found in many papers, such as research work [29], where few saturated nonlinear functions are presented. Moreover, realizations given in this paper are ready for integration using CMOS technology and resistant against process, voltage, and temperature variations.

Speaking in terms of analog implementation of the chaotic system, field programmable analog array (FPAA) provides many benefits over those realizations with discrete electronic components. The main advantage of FPAA is fast realization of a chaotic oscillator since commercially available platforms provide users with all necessary building blocks. Problem associated with FPAA-based design is inevitable low pass filtering effect applied on the state variables and a limited workspace dedicated for realization of the circuit schematic. Because of a broadband nature of the chaotic signals, roll-off effects can cause serious deformation and/or disappearing of prescribed strange attractors. Technical and implementation details including interesting practical examples can be found in paper [30] or book [31], where particular attention of the authors is paid on design of fractional-order chaotic systems.

Field programmable gate array (FPGA) can be utilized as the bridge between software-oriented numerical investigation of nonlinear differential equations and its practical realization in the form of lumped electronic circuit. Main advantage of FPGA-based design of the chaotic system is fast prototyping, high processing speed, and programming flexibility. Design process starts with discretization of all differential equations, difference equations are subsequently iterated using available building blocks in frame of workplace of a development kit. Therefore, all outputs coming from FPGA realization still belong to simulation results, more likely related to numerical integration process in mathematical environment rather than connected with real measurement. Several interesting papers can be addressed for more details about FPGA-based design, for example [32]–[36].

When studying global dynamics associated with naturally linear analog functional blocks, chaotic motion was revealed as surprising and unexpected, but observable phenomena in many cases. For example, standard structures of frequency filters can generate robust driven chaotic waveforms [37], [38]. Power electronic could provide enough degrees of freedom and functional nonlinearities required for evolution of chaos. Let us mention discovery of irregular behavior of dc-dc [39] and buck [40] converters, switched-mode power converters [41], switching boost regulators [42], and many others. Switching or, more generally speaking, repeated change of circuit topology, can also lead to the robust chaotic behavior. Chaotic attractors were reported from the switched capacitor networks [43]. Spiral strange attractors evolved within static multi-state memory system composed by series or parallel connection of two resonant tunneling diodes was described very recently [44]. To mention final example of chaos inside system that is originally non-chaotic, research papers [45], [46] demonstrate such regimes in the case of phase locked loops with realistic values of all circuit components.

Few recent papers were focused on the problem of a robust chaos localization in analog electronic systems containing the so-called generalized bipolar transistor (GBT). This active device is modelled by equivalent two-port described by 2×2 admittance matrix where input y_{11} and output y_{22} admittance is positive constant. Both forward y_{21} and backward y_{12} trans-conductance are considered as nonzero and could be scalar nonlinear functions. The latter property is assumed in paper [47] where $y_{21}(v_1)$ and $y_{12}(v_2)$ are cubic polynomial functions and single GBT-based amplifier is addressed. New shapes of the chaotic attractors are reported also for the case where y_{21} is linear and $y_{12}(v_2)$ is the only nonlinearity. More details can be found in work [48]. From the viewpoint of real situation, only forward trans-conductance $y_{21}(v_1)$ should be considered as a saturation-type nonlinear function. This restriction does prevent analyzed circuit to behave chaotically, as pointed out in paper [49]. Important finding coming from these works is existence of chaos itself. Admittance parameters leading to complex behavior are far away from the standard operational state of bipolar transistor. Presence of GBT does not simplify design process of the chaotic oscillator, neither composed by discrete components nor its on-chip integrated version.

This paper is organized as follows. Next section introduces mathematical model that arises from two-stage amplifier with common-emitter generalized bipolar transistors. Third part is focused on chaotification process, while fourth section brings numerical analysis of mentioned dynamic system, especially to demonstrate evidence of strange attractor. It is shown that chaos is neither numerical artifact nor long transient motion. Standard forms of behavior quantification are given, namely Lyapunov exponents (LE), Kaplan-Yorke dimension (KYD), bifurcation diagrams (BD) calculated via Poincare sections, basins of attraction (BoA), kinetic energy distribution (KED) over the state space, sensitivity analysis, etc. Of course, these routines still deal with normalized numerical values of the internal system parameters. Fifth part of this work describes

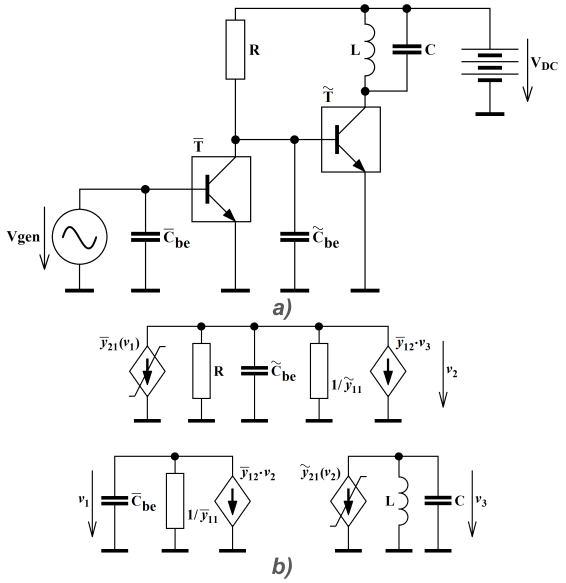

FIGURE 1. Simplified schematic of analyzed networks: a) concept of driven two-stage class C amplifier with generalized bipolar transistors, b) isolated circuit with equivalent models of generalized transistors.

circuit realization of chaotic oscillator based on mathematical model of the two-stage cascaded class C amplifier. From this place further, the real-valued passive circuit components are addressed. Sixth section covers experimental confirmation of chaos in a designed hyperchaotic oscillator and contains rich gallery of oscilloscope screenshots. Some of these are put into context of previously discussed numerical investigation. Finally, concluding remarks, discussion of achieved results and future research topics are stated.

II. TOPOLOGY OF TWO-STAGE CLASS C AMPLIFIER

Fundamental circuit topology of a two-stage amplifier based on cascade connection of two generalized bipolar transistors (GBT) is shown in Fig. 1a. Transistors use common emitter topology and circuit is loaded by a parallel LC resonant tank. As already mentioned above, each GBT cell is electrically modeled by the following set of the components of two-port admittance matrix: constant positive input admittance y_{11}, output admittance y_{22} equals to zero, linear backward transconductance $y_{12}(v_{CE})$, and a scalar nonlinear forward transconductance $y_{21}(v_{BE})$ having a cubic polynomial form

$$y_{21}\left(v_{be}\right) = a \cdot v_{be}^3 + b \cdot v_{be}, \tag{1}$$

where a and b are real numbers and v_{be} is immediate voltage between base and emitter. In upcoming text, line and wavelet above admittance parameter means that it is associated with first and second GBT, respectively. Considering equivalent circuit given in Fig. 1b following set of first order ordinary differential equations can be derived

$$\begin{aligned}
\bar{C}_{be}\frac{d}{dt}v_1 &= -\bar{y}_{11}\cdot v_1 - \bar{y}_{12}\cdot v_2,\\
\tilde{C}_{be}\frac{d}{dt}v_2 &= -\tilde{y}_{21}\left(v_1\right) - \left(\tilde{y}_{11}+\frac{1}{R}\right)\cdot v_2 - \tilde{y}_{12}\cdot v_3,\\
C\frac{d}{dt}v_3 &= -\tilde{y}_{21}\left(v_2\right) - i_L, L\frac{d}{dt}i_L = v_3.
\end{aligned} \tag{2}$$

Four element vector of the state variables is $\mathbf{x} = (v_1, v_2, v_3, i_L)^{\mathrm{T}}$. Symbols y_{ik} in equations (2) supplemented by line and wave represent the admittance parameters associated with first and second GBT respectively.

Note that amplifier is analyzed as isolated, that is without input signal. Analysis of linearized autonomous deterministic dynamical system (2) starts with a determination of the fixed points. There is always one equilibrium located at the origin, that is $\mathbf{x}_0 = (0, 0, 0, 0)^{\mathrm{T}}$. Other fixed points exist only under condition of positive value of square root in formula (3), and these are located at

$$\boldsymbol{x}_0 = \left(\pm\sqrt{\frac{\vartheta-\bar{b}}{\bar{a}}}, \mp\frac{\bar{y}_{11}}{\bar{y}_{12}}\sqrt{\frac{\vartheta-\bar{b}}{\bar{a}}}, 0, -\tilde{y}_{21}\cdot\beta\right)^T, \tag{3}$$

where first auxiliary parameter is

$$\vartheta = \bar{y}_{11}\left(\tilde{y}_{11}+1/R\right)/\bar{y}_{12}, \tag{4}$$

and second equals

$$\beta = \mp\tilde{a}\left(\frac{\vartheta-\bar{b}}{\bar{a}}\right)^{\frac{3}{2}} \mp\sqrt{\frac{\vartheta-\bar{b}}{\bar{a}}}. \tag{5}$$

Linearization matrix calculated around fixed points can be expressed as

$$\boldsymbol{J}\left(\boldsymbol{x}_0\right) = \begin{pmatrix} -\frac{\bar{y}_{11}}{\bar{C}_{be}} & -\frac{\bar{y}_{12}}{\bar{C}_{be}} & 0 & 0\\ -\frac{3\cdot\tilde{a}\cdot x_0^2+\tilde{b}}{\tilde{C}_{be}} & -\frac{\tilde{y}_{11}+1/R}{\tilde{C}_{be}} & -\frac{\tilde{y}_{12}}{\tilde{C}_{be}} & 0\\ 0 & -\frac{3\cdot\tilde{a}\cdot y_0^2+\tilde{b}}{C} & 0 & -\frac{1}{C}\\ 0 & 0 & \frac{1}{L} & 0 \end{pmatrix}. \tag{6}$$

From the viewpoint of chaos evolution, fixed point located at origin plays a crucial role. Local dynamical behavior in the close neighborhood of equilibrium points is defined by the eigenvalues, i.e., roots of polynomial

$$\begin{aligned}
&det\left[\lambda\cdot\boldsymbol{E}-\boldsymbol{J}\left(\boldsymbol{x}_0\right)\right]\\
&=\lambda^4+\left(\frac{1}{\tilde{C}_{be}\cdot R}+\frac{\tilde{y}_{11}}{\tilde{C}_{be}}+\frac{\bar{y}_{11}}{\bar{C}_{be}}\right)\lambda^3\\
&+\left(\frac{1}{L\cdot C}-\frac{\bar{y}_{12}\cdot\left(3\cdot\tilde{a}\cdot x_0^2+\tilde{b}\right)+\bar{y}_{11}\left(\tilde{y}_{11}-1/R\right)}{\bar{C}_{be}\cdot\tilde{C}_{be}}\right.\\
&\left.-\frac{\tilde{y}_{12}\cdot\left(3\cdot\tilde{a}\cdot y_0^2+\tilde{b}\right)}{\tilde{C}_{be}\cdot C}\right)\lambda^2+\left(\frac{1}{\tilde{C}_{be}\cdot C\cdot L\cdot R}\right.\\
&\left.+\frac{\tilde{y}_{11}}{\tilde{C}_{be}\cdot C\cdot L}+\frac{\bar{y}_{11}}{\bar{C}_{be}\cdot C\cdot L}-\frac{\bar{y}_{11}\cdot\tilde{y}_{12}\cdot\left(3\cdot\tilde{a}\cdot y_0^2+\tilde{b}\right)}{\bar{C}_{be}\cdot\tilde{C}_{be}\cdot C}\right)\\
&\times\lambda+\frac{\bar{y}_{11}+R\cdot\left(\bar{y}_{11}\cdot\tilde{y}_{12}-\bar{y}_{12}\cdot\left(3\cdot\tilde{a}\cdot x_0^2+\tilde{b}\right)\right)}{\bar{C}_{be}\cdot\tilde{C}_{be}\cdot C\cdot L\cdot R}=0,
\end{aligned} \tag{7}$$

where $\mathbf{E}$ is square unity matrix, x_0 and y_0 is first and second coordinate of the fixed point, respectively. To symbolically evaluate the eigenvalues, Cardan rules should be addressed. However, continuation with linear analysis is pointless since symbolic formulas for individual eigenvalues are enormously

complex and cannot be even displayed using math software. Thus, a significant simplification should be introduced before starting optimization problem that will result into structurally stable chaotic nature of two-stage class C amplifier.

III. AMPLIFIER CHAOTIFICATION PROCESS

Procedure of dynamical system chaotification is dedicated to find numerical values of internal system parameters such that system exhibits following features simultaneously: bounded ω-limit set, self-excited and dense strange attractor with non-integer geometrical dimension. Since there is no closed-form analytic solution of the chaotic system chaotification can be considered as numerical problem of multi-criteria stochastic optimization. Fortunately, individual fitness functions can be calculated separately using specific set of initial conditions as well as internal system parameters, both defined as the vector global parameters.

Interesting approach how to deal with a chaos localization problem is suggested in paper [50] where two-step procedure is suggested. Proposed optimization method can be marked as metaheuristic, combines differential evolution and particle swarm optimization. First step is evaluation of fixed points and associated eigenvalues and is applied on each population individual. Those solution that satisfies prescribed ''chaotic assumptions'' pass to second step, calculation of KYD. In this paper, authors focus on the fractional-order chaotic dynamic. Therefore, useful information about this kind of a dynamical motion can be found [50] and references given therein.

Note that at this moment analyzed circuit contains thirteen free parameters $\left\{\bar{C}_{be}, \tilde{C}_{be}, C, R, L, \bar{y}_{11}, \bar{y}_{12}, \bar{a}, \bar{b}, \tilde{y}_{11}, \tilde{y}_{12}, \tilde{a}, \tilde{b}\right\}$. Each parameter represents one dimension in a hyperspace of system parameters dedicated for optimization routine. This is huge number of combinations for a full grid calculation, even for the CUDA-based parallel processing using Matlab. Thus, investigated hyperspace needs to be significantly reduced by introducing additional assumptions and restrictions. None of these, of course, should prevent optimized dynamical system to behave chaotically. First restriction is related to uniform normalized values of accumulation elements. Such choice is equivalent to set a multiplication factor for each differential equation to one. Values $\bar{C}_{be} = \tilde{C}_{be} = C = 1F$ and $L = 1$ H still allow us to observe chaotic motion while hyperspace is reduced to have nine edges. Secondly, resistor R can be removed since proper bias point set is covered by two-port admittance parameters, that is without the necessity to solve biasing circuitry. Third assumption is based on reachability of prescribed local vector field geometry near fixed point at origin, namely a saddle spiral movement. It can be shown that the equality $\bar{y}_{12} = \tilde{y}_{12}$ together with $\bar{a} = \tilde{a}$ fulfill this condition. Substitution of the state coordinates $x_0 = y_0 = 0$ leads to the characteristic polynomial (7) in simplified form

$$\lambda^4 + (\bar{y}_{11} + \tilde{y}_{11})\,\lambda^3 + \left[\bar{y}_{11} \cdot \tilde{y}_{11} - \bar{b} - \tilde{b} + 1\right]\lambda^2 + \left[\tilde{y}_{11} + \bar{y}_{11}\left(1 - \tilde{b}\right)\right]\lambda + \bar{y}_{11} - \bar{b} = 0. \quad (8)$$

Obviously, hyperspace of free internal system parameters is six-dimensional now. This is reasonable level of complexity where robust chaotic behavior can be successfully detected, the most probably next to the limit cycle solution. Instability of fixed point at origin, boundness of attractor, and sensitive dependance on initial condition are three objective functions that need to be satisfied simultaneously. Unfortunately, the full-grid calculation toward robust chaotic solution is still too time consuming. As the main search engine, CUDA-powered genetic algorithm was utilized. In contrast with paper [50], where individuals in population are in fact removed if carry parameter values that does not meet ''chaotic assumptions'', objective function receives serious penalization in the case of violation of conditions mentioned above.

Detail calculation discovers several topologically different chaotic and hyperchaotic cases of mathematical model (2). Let denote following set of the internal parameters that leads to distinguished hyperchaotic motion as case one, namely

$$\bar{y}_{11} = 0.5, \quad \bar{y}_{12} = \tilde{y}_{12} = 1, \quad \tilde{y}_{11} = 0.3, \quad \bar{a} = \tilde{a} = -2, \quad \bar{b} = 5, \quad \tilde{b} = 4. \quad (9)$$

For this numerical set, eigenvalues associated with origin are $\lambda_1 = -3.25$, $\lambda_2 = 2.63$, $\lambda_{3,4} = -0.09 \pm \mathrm{j}0.75$ and this corresponds to the composition of spiral movement along two-dimensional stable manifold and two-dimensional saddle-node.

Case two can be obtained for following set of the internal parameters of GBT

$$\bar{y}_{11} = 0, \quad \bar{y}_{12} = \tilde{y}_{12} = 1, \quad \tilde{y}_{11} = 0.5, \quad \bar{a} = \tilde{a} = -2, \quad \bar{b} = 5, \quad \tilde{b} = 4. \quad (10)$$

For this numerical set, eigenvalues associated with origin are $\lambda_1 = -3.20$, $\lambda_2 = 2.68$, $\lambda_{3,4} = 0.01 \pm \mathrm{j}0.76$, i.e., it is combination of spiral movement along unstable (with slow repelling nature) eigen-plane and two-dimensional saddle-node.

To this end, the last interesting set of internal parameters worthy for more detailed analysis is

$$\bar{y}_{11} = 0, \quad \bar{y}_{12} = \tilde{y}_{12} = 1, \quad \tilde{y}_{11} = 0.01, \quad \bar{a} = \tilde{a} = -2, \quad \bar{b} = 5, \quad \tilde{b} = 4. \quad (11)$$

For this numerical set, eigenvalues associated with origin are $\lambda_1 = -2.94$, $\lambda_2 = 2.92$, and $\lambda_{3,4} = \pm \mathrm{j}0.76$, which is combination of circular move and two-dimensional saddle-node geometry. This situation will be referred as third case.

IV. NUMERICAL RESULTS

All numerical procedures presented in this paper are based on fourth order Runge-Kutta integration method with fixed step size. Figure 2 provides typical strange attractor generated by dynamical system (2) with parameter set (9) in available cube projections. Figure 3 provides the same meaning plots but for dynamical system (2) having second set of parameters (10). Figure 4 shows available three-dimensional projections of the typical strange attractor generated by dynamical system (2) having set of internal parameters (11). Although generated by

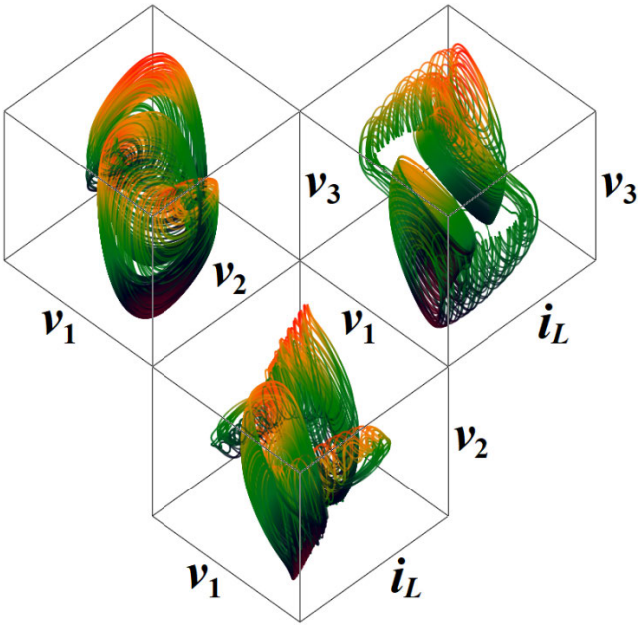

FIGURE 2. Three-dimensional colored cube projections of typical strange attractor generated by analyzed dynamical system, first case.

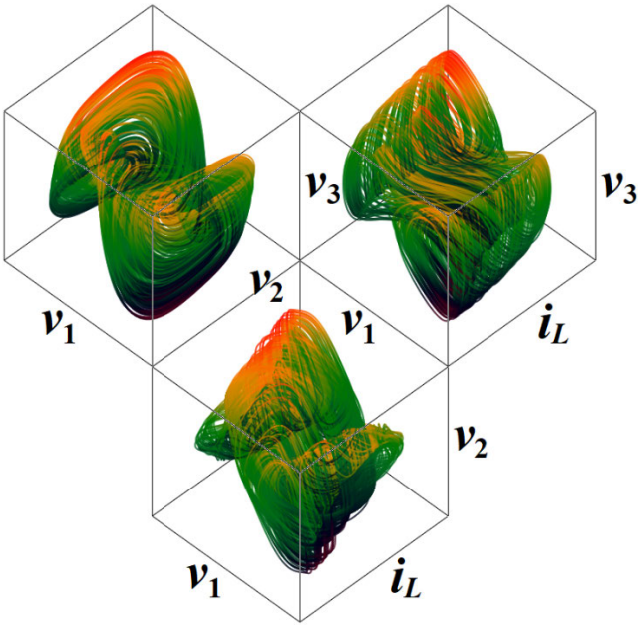

FIGURE 3. Three-dimensional colored cube projections of typical strange attractor generated by dynamical system (2), second case.

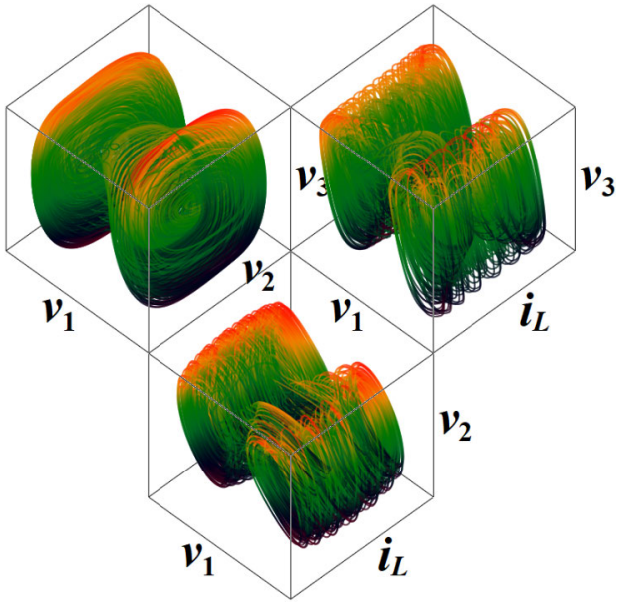

FIGURE 4. Three-dimensional colored cube projections of typical strange attractor generated by dynamical system (2), third case.

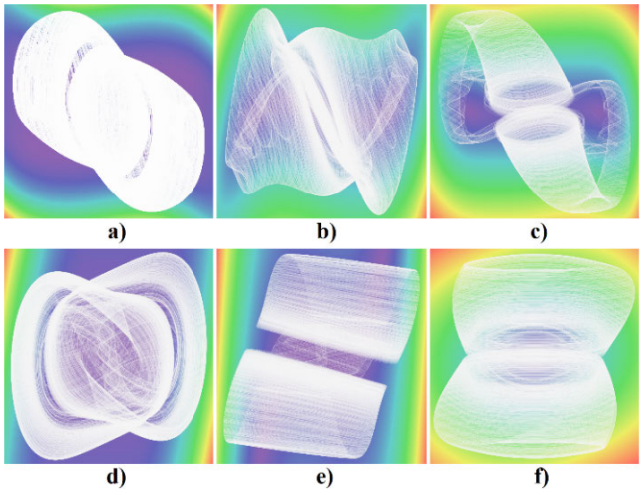

FIGURE 5. Plane projections of typical chaotic attractor and surface calculation of kinetic energy distribution, ranges for state variables are $v_1 \in(-2.6, 2.6)$ V, $v_2 \in(-4.5, 4.5)$ V, $v_3 \in(-15.2, 15.2)$ V and $i_L \in(-26, 26)$ A: a) v_1 vs v_2, b) v_1 vs v_3, c) v_1 vs i_L, d) v_2 vs v_3, e) v_2 vs i_L, f) v_3 vs i_L.

the same mathematical model, geometrical shapes of strange attractors are different. All state trajectories mentioned above were integrated using the same set of input parameters, i.e., set of initial conditions $\mathbf{x}_0 = (0.1, 0, 0, 0)^{\mathrm{T}}$, final time 1000 s and time step 10 ms.

Figure 5, 6 and 7 show rainbow-scaled KED over the state space limited to volume that is occupied by chaotic attractor. Individual image results are tied with dynamical system (2) having parameter group (9), (10) and (11) respectively. Plots of energy are calculated with 0.1 s time instant and steps of state variables 0.01. In these plots, red denotes high dynamic energy, green color marks area with the average speed and magenta represents areas with low move gradient. Note that chaotic attractor is placed in a state space region with low gradient, surrounded by area of strong four-dimensional state space volume expansion, that is where kinetic energy is very high. Also, it seems that the colored patterns for individual parameter cases are similar.

Figure 8 demonstrates sensitivity of chaotic system to tiny change of 10^4 initial states with normal distribution generated around nominal value $\mathbf{x}_0 = (-1, -2, 0, 0)^{\mathrm{T}}$, standard deviation is chosen 0.1. These starting points are marked by green color. As system evolves, states after 100 s are stored as red

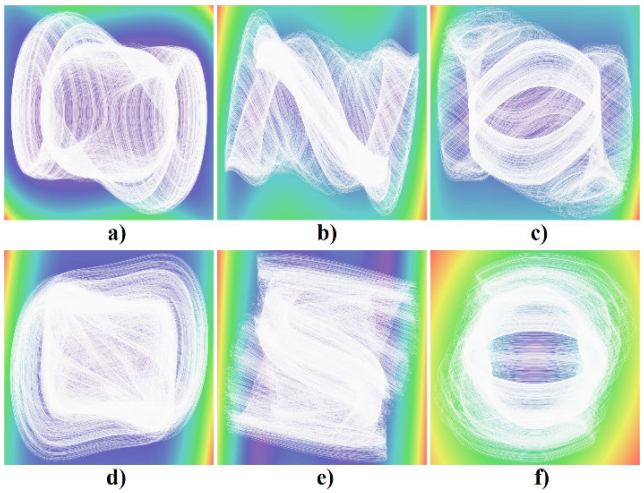

FIGURE 6. Plane projections of typical chaotic attractor and associated surface calculation of kinetic energy distribution in following ranges: $v_1 \in(-2.5, 2.5)$ V, $v_2 \in(-3.3, 3.3)$ V, $v_3 \in(-8.5, 8.5)$ V, and $i_L \in(-8.5, 8.5)$ A. Plots: a) v_1 vs v_2, b) v_1 vs v_3, c) v_1 vs i_L, d) v_2 vs v_3, e) v_2 vs i_L, f) v_3 vs i_L.

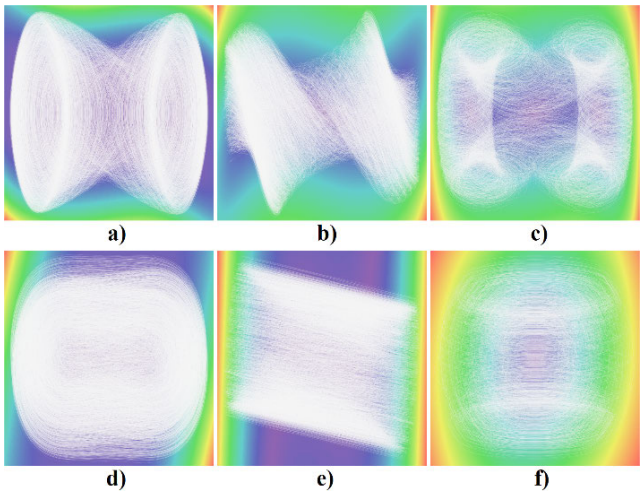

FIGURE 7. Plane projections of typical chaotic attractor and associated surface calculation of kinetic energy distribution for state variables ranges $v_1 \in(-2.5, 2.5)$ V, $v_2 \in(-3.3, 3.3)$ V, $v_3 \in(-8.5, 8.5)$ V, $i_L \in(-8.5, 8.5)$ A. Plots: a) v_1 vs v_2, b) v_1 vs v_3, c) v_1 vs i_L, d) v_2 vs v_3, e) v_2 vs i_L, f) v_3 vs i_L.

points and final states after 1000 s of system evolution are denoted by blue color. All plots have equally scaled axis system. This figure contains all available cube projection of this sensitivity effect. Also, both plots visually suggest quite fast divergence ratio between two neighborhood trajectories in the state space and expects quite high values of the positive LE.

Figure 9 thoroughly analyzes dynamical system (2) in the close neighborhood of parameter set (9) from the viewpoint of chaotic and hyperchaotic solution. Both LE and KYD is calculated via Matlab, routine for both 3D and 4D dynamical systems are very similar and differs only in sizes of Jacobi matrices, state vectors and dimension of used Gram-Smith orthogonalization. Numerical values of LE and KYD were calculated for data sequence ending with 10^4 s and the initial

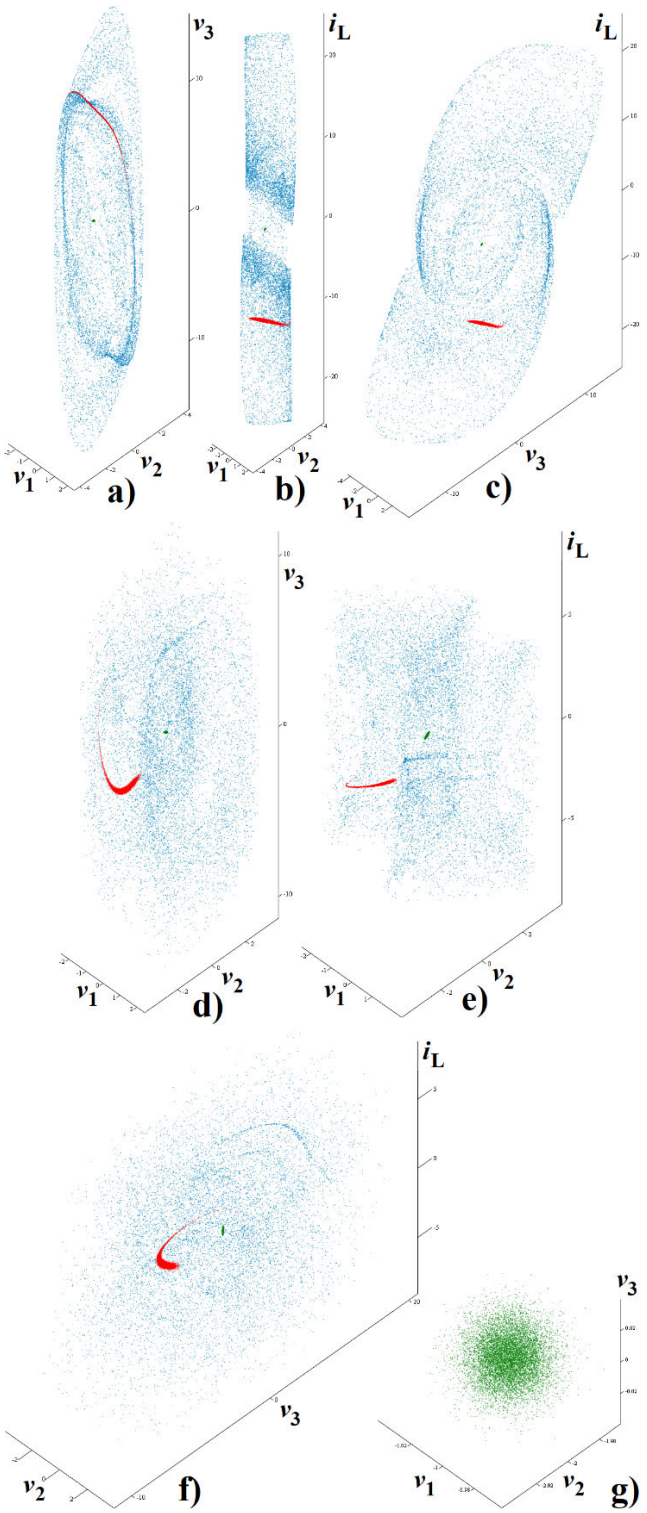

FIGURE 8. Graphical demonstration of chaotic system sensitivity to the uncertainties in the initial conditions, see text for better clarification. Individual three-dimensional projections are associated with analyzed dynamical system (2) with: a) b) c) parameter group (9) and different cube projections, d) e) f) parameter group (11) and available cube projections, g) distribution of randomly generated initial conditions visualized in cube v_1-v_2-v_3.

conditions randomly placed near repelling fixed point located at origin. Procedure used for calculation of LE can be found

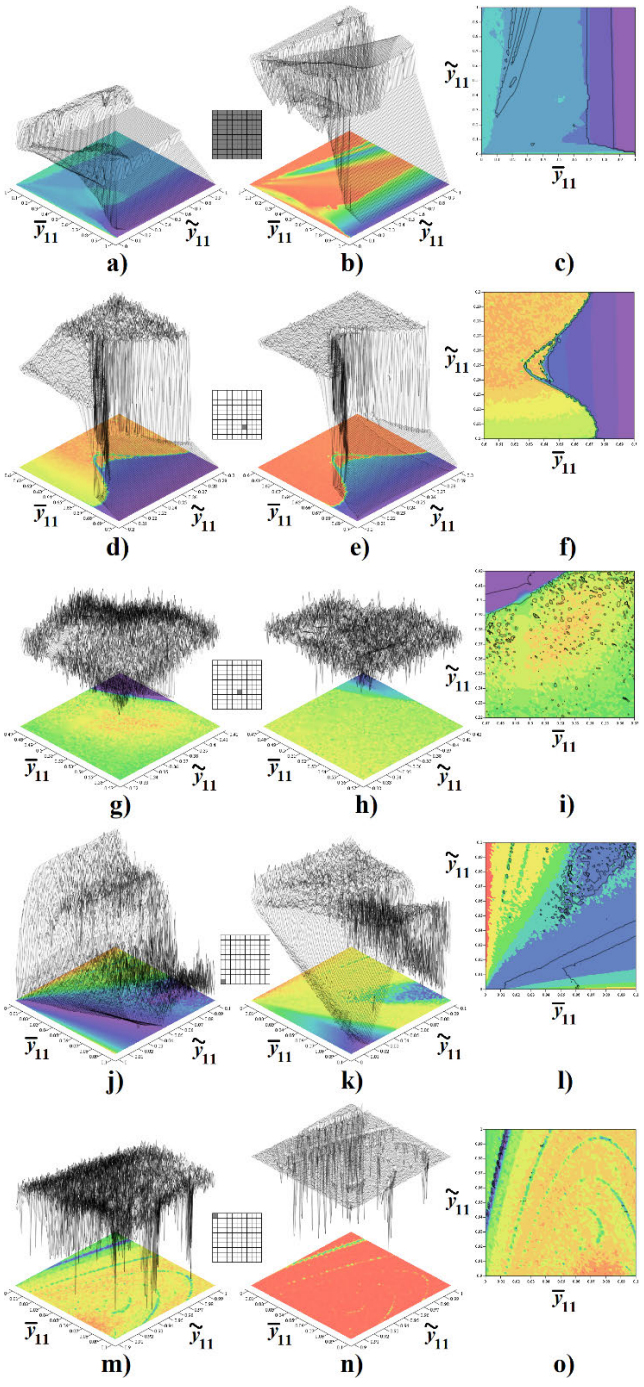

FIGURE 9. Rainbow-scaled surface-contour plot of two largest LE as function of input admittances of GBT near to the nominal values (9), range of both admittances 0 S up to 1 S: a) the largest LE, b) second LE, c) intersection of chaotic and hyperchaotic areas. Zoomed area focused on range 600 mS to 700 mS of first GBT vs 200 mS to 300 mS of second GBT: d) the largest LE, e) second LE, f) intersection of chaos and hyperchaos. Zoomed area aimed on range 470 mS to 570 mS of first GBT vs 320 mS to 420 mS of second GBT's: g) the largest LE, h) second LE, i) boundaries for chaotic and hyperchaotic motion. Magnified region 0 S to 100 mS of first GBT vs 0 mS to 100 mS of second GBT: j) the largest LE, k) second LE, l) boundaries for chaotic and hyperchaotic system behavior. Magnified area focused on range 0 S to 100 mS of first GBT vs 900 mS to 1 S of second GBT: m) the largest LE, n) second LE, o) boundaries evaluated for chaotic and hyperchaotic system behavior.

in detailed book [51]. Curious readers that are interested in the algorithmizing and routine verification, paper [52] could be recommended to see. In accordance with the known math definitions, both first and second LE (sorted in descending order) need to be distinguishably positive for hyperchaotic behavior. That is why contour plots contour plots in Fig. 9c), f), i), l), and o) are provided: the colored areas correspond to the largest LE while limited number of the black contours (3) specify various numerical levels of second LE (positive, zero, negative). Details involving qualitative analysis of dynamical behavior can be found in paper [53]. For nominal numerical value set (9) dynamical system (2) is "only" chaotic since second LE is close to zero and KYD is $D_{KY} = 2.31$. In frame of this investigation, "the most chaotic" strange attractor was observed by a computer-aided analysis of dynamical system (2) together with numerical value set (11) leading to KYD about $D_{KY} = 3.78$. Therefore, we are experiencing very strong hyperchaos with a very short time instance with predictable dynamical evolution. It should be noted that the hyperchaotic motion is by no way ordinary or obvious solution. It is quite rare property often associated with the higher-order nonlinear dynamical systems. However, mathematical model analyzed in this paper exhibits very large areas of the internal system parameters with associated hyperchaotic motion.

A. ALGEBRAICALLY SIMPLEST CASE

Proposed optimization/searching algorithm can be employed to find the simplest mathematical model (2) that still exhibits chaotic and/or hyperchaotic behavior. For example, set of the internal parameters

$$\begin{aligned} \bar{y}_{11} = 0, \quad \bar{y}_{12} = 0.55, \quad \tilde{y}_{11} = 0, \quad \tilde{y}_{12} = 1, \\ \bar{a} = \tilde{a} = -2, \quad \bar{b} = 5, \quad \tilde{b} = 4. \end{aligned} \tag{12}$$

leads to hyperchaotic behavior for different choices of initial conditions, such as $\mathbf{x}_0 = (0.1, 0, 0, 0)^{\mathrm{T}}$. Few graphical results are provided in Fig. 10. It can be easily proved that origin is unstable fixed point and local vector field is characterized by eigenvalues $\lambda_1 = -\lambda_2 = 2.49$ and $\lambda_{3,4} = \pm \mathrm{j}0.67$, i.e., local behavior is combination of center and saddle-node kind of movement. This flow is highly unpredictable due to expressive values of first two LE (0.135 and 0.023). Both LEs are positive such that dynamical evolution belongs to a hyperchaotic behavior. Existence of many robust state attractors associated with this case of dynamical system is geometrically demonstrated via Fig. 11. In these plots, initial conditions differ only in a state coordinate x_0, the rest of initial states are zero. Thus, basins of attraction are complicated geometrical structures, crawled with each other. Calculation of KYD reveals that observable ω-limit sets have different metric dimensions.

Coexistence of several qualitatively different solutions can cause problems in the task of experimental verification, i.e., confirmation of physical presence of desired strange attractor

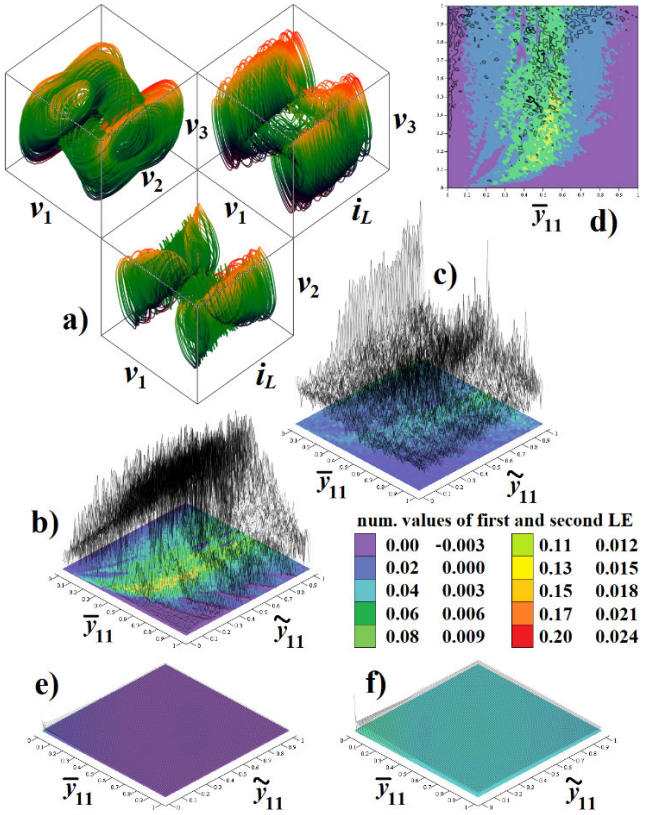

FIGURE 10. Numerical analysis of dynamical system (1) with zero input admittances of both GBT: a) discovered strange attractor, b) the largest LE, c) second LE, d) intersection of chaotic and hyperchaotic regions. Rainbow scaled surface-contour plot of LE for zero backward trans-conductances of both GBT: e) first LE, f) second LE.

produced by designed chaotic oscillator can be complicated. Vector field symmetry is invariant under the flow initiated by system (2) and is illustrated via visualized state trajectories in Fig. 11 as well.

On the other hand, searching for chaotic solution was not successful if backward trans-conductances of both GBT are assumed zero. Origin becomes stable equilibria attracting all neighborhood trajectories with exception of those settling on the center manifold. Such situation is closely related to a real circuitry with bipolar transistors.

However, the so-called hidden chaotic attractors [54], [55] cannot be eliminated from the gallery of possible solutions of dynamical system (2). This kind of computationally intensive numerical investigation can be considered as good topic for future research.

B. OTHER INTERESTING CHAOTIC CASES

Many interesting, strange state attractors can be observed for other choices of the internal parameters associated with GBT. For example, following set

$$\bar{y}_{11} = 0.5, \quad \bar{y}_{12} = 1, \quad \tilde{y}_{11} = 0.3, \quad \tilde{y}_{12} = 0.4,$$
$$\bar{a} = \tilde{a} = -2, \quad \bar{b} = 5, \quad \tilde{b} = 4, \tag{13}$$

leads to chaotic behavior visualized in Fig. 12 for wide area of the initial states, for example $\mathbf{x}_0 = (-1.8, 0, 0, 5)^{\mathrm{T}}$.

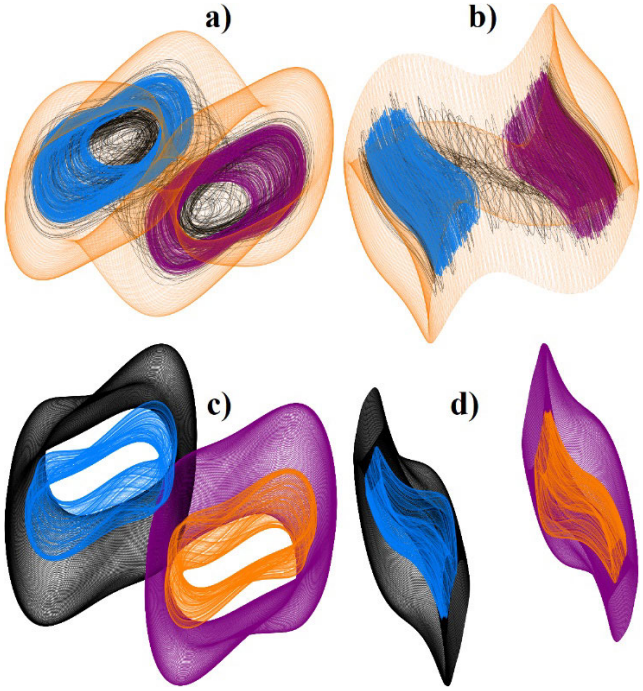

FIGURE 11. Existence of several state attractors within dynamical system (2) with a group of parameters (12), v_1 vs v_2 vs v_3 projections for: a) b) $x_0 = 0.1$ (black), $x_0 = 0.3$ (purple), $x_0 = -0.3$ (blue), $x_0 =$(orange), c) d) $x_0 = -0.8$, $x_0 = 0.8$ (purple), $x_0 = -2$ (blue), and $x_0 = 2$ (orange).

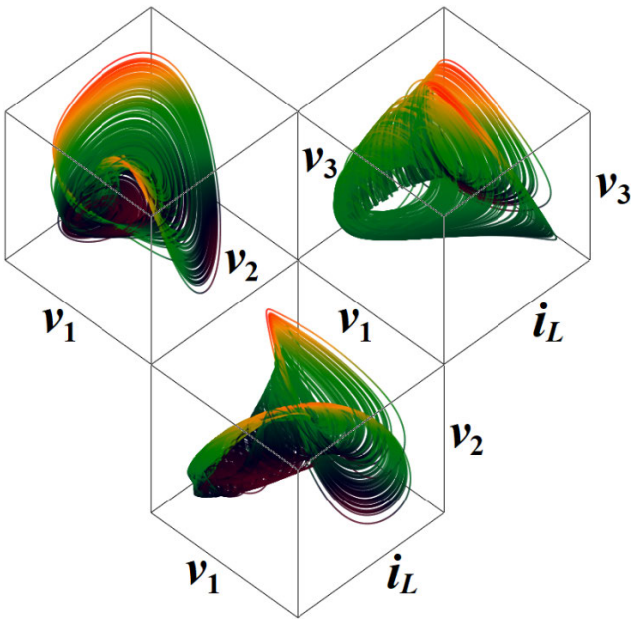

FIGURE 12. Three-dimensional colored cube projections of typical strange attractor generated by dynamical system (2) with set (13).

Fixed point located at the origin is the unstable equilibria and local dynamical flow is uniquely determined by the eigenvalues $\lambda_1 = -3.05$, $\lambda_2 = 2.25$ and $\lambda_{3,4} = \pm \mathrm{j}$. Observed global dynamical motion can be marked as chaotic and is characterized by the Kaplan-Yorke dimension $\mathrm{D_{KY}} = 2.25$. By adopting following set of internal system

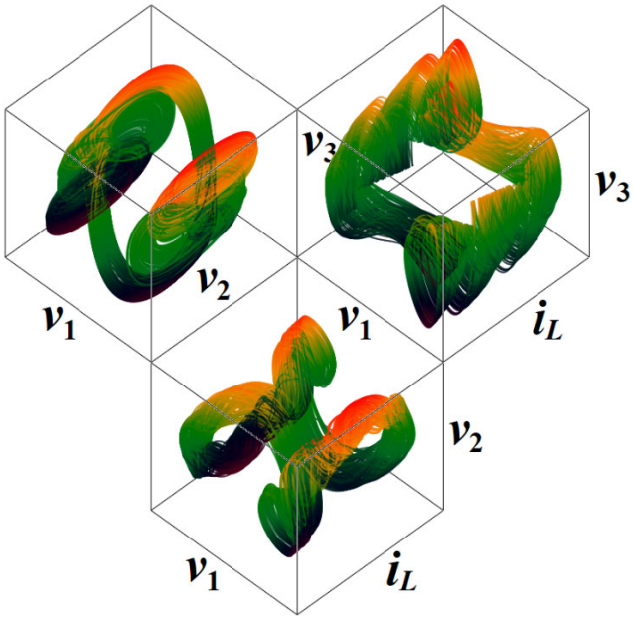

FIGURE 13. Three-dimensional colored cube projections of typical strange attractor generated by dynamical system (2) with set (14).

parameters

$$\bar{y}_{11} = 0, \quad \bar{y}_{12} = 1, \quad \tilde{y}_{11} = 0.3, \quad \tilde{y}_{12} = 1,$$
$$\bar{a} = \tilde{a} = -2, \quad \bar{b} = 7, \quad \tilde{b} = 0, \tag{14}$$

together with set of the initial conditions $\mathbf{x}_0 = (1, 0, -7, -5)^{\mathrm{T}}$ unconventional attractor depicted in Fig. 13 can be observed. Again, origin is unstable equilibria and local dynamical flow is characterized by eigenvalues $\lambda_1 = 2.5$, $\lambda_2 = -2.8$ and $\lambda_{3,4} = \pm \mathrm{j}$. In this case, system (2) is chaotic with spectrum of the one-dimensional LE (0.1421, 0, –0.138, –0.3032) and $D_{KY} = 3.32$.

V. DESIGN OF CHAOTIC OSCILLATORS

With the knowledge of complete mathematical description of dynamical system (both equations and parameters), synthesis of lumped electronic circuit is easy and straightforward task. In this section, two interesting cases of dynamical system (2) will be implemented: with parameter set (12) and using value set (14). Thus, upcoming two systems of ordinary differential equations, normalized with respect to both frequency and impedance, will be considered

$$\frac{d}{dt}v_1 = -0.55 \cdot v_2, \; \frac{d}{dt}v_2 = 2 \cdot v_1^3 - 5 \cdot v_1 - v_3,$$
$$\frac{d}{dt}v_3 = 2 \cdot v_2^3 - 4 \cdot v_2 - v_4, \; \frac{d}{dt}v_4 = v_3, \tag{15}$$

and

$$\frac{d}{dt}v_1 = -v_2, \; \frac{d}{dt}v_2 = 2 \cdot v_1^3 - 7 \cdot v_1 - 0.3 \cdot v_2 - v_3,$$
$$\frac{d}{dt}v_3 = 2 \cdot v_2^3 - v_4, \; \frac{d}{dt}v_4 = v_3. \tag{16}$$

First circuit realization is provided by means of Fig. 14. Straightforward analysis yields following set of differential

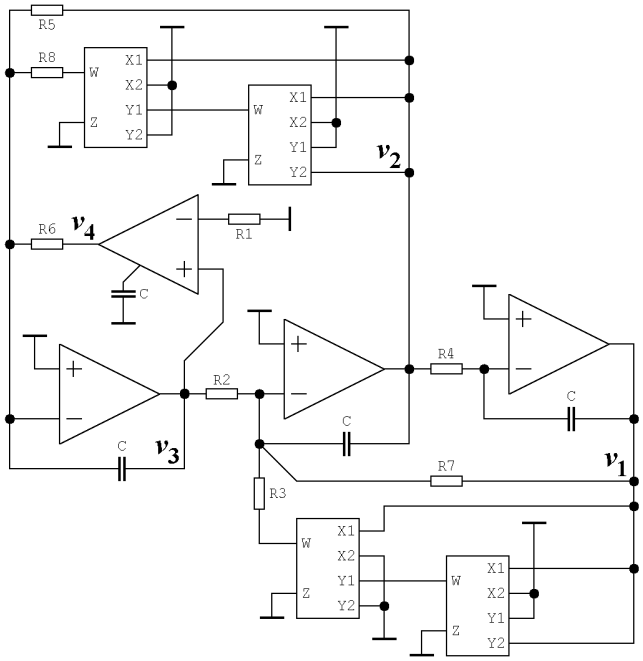

FIGURE 14. Circuitry implementation of dynamical system (17) with real circuit components, i.e., after frequency and impedance rescaling.

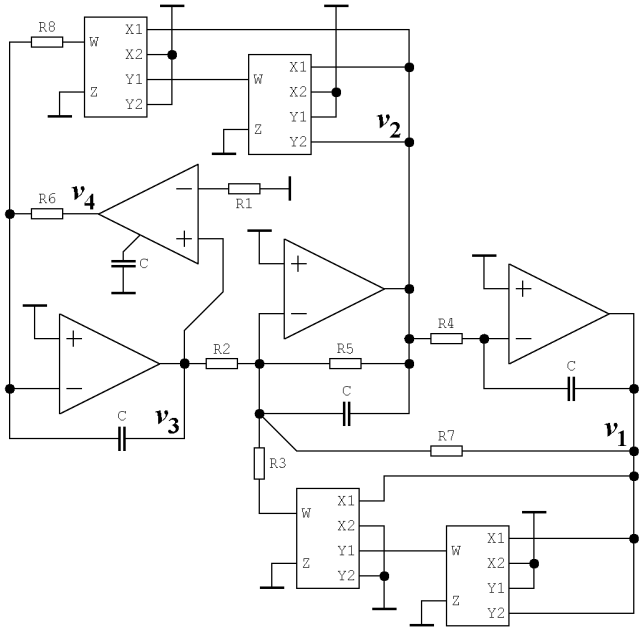

FIGURE 15. Practical circuit realization of dynamical system (18) with real, denormalized circuit components.

equations that describe its behavior

$$\frac{d}{dt}v_1 = -\frac{1}{R_4 C}v_2, \quad \frac{d}{dt}v_2 = -\frac{1}{R_7 C}v_1 - \frac{1}{R_2 C}v_3 + \frac{K^2}{R_3 C}v_1^3,$$
$$\frac{d}{dt}v_3 = -\frac{1}{R_5 C}v_2 - \frac{1}{R_6 C}v_4 + \frac{K^2}{R_8 C}v_2^3, \quad \frac{d}{dt}v_4 = \frac{1}{R_1 C}v_3, \tag{17}$$

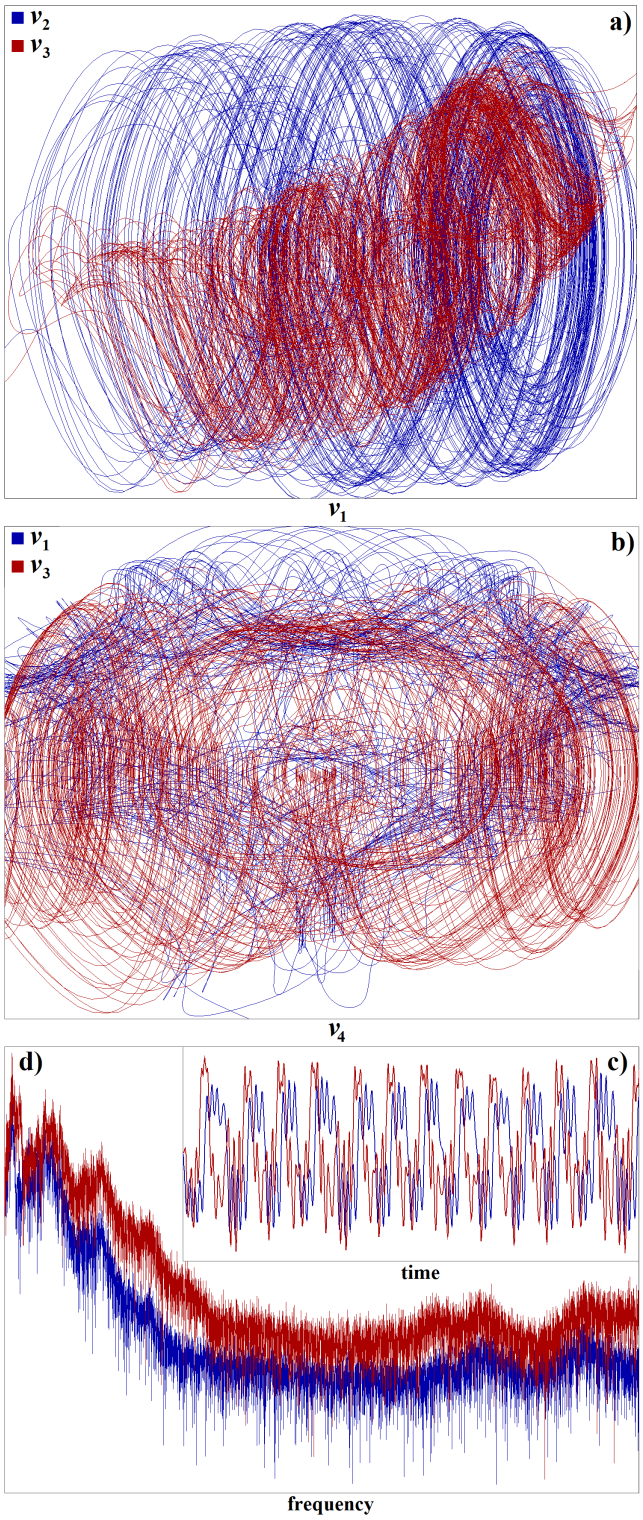

FIGURE 16. Orcad Pspice circuit simulation of dynamical system (17), ranges of the state variables: a) horizontal axis $v_1 \in$(600 mV, 2.2 V), vertical scale $v_2 \in$(−3 V, 3 V), and $v_3 \in$(−10 V, 10 V), b) horizontal axis $v_4 \in$(−11 V, 9 V), vertical scale is $v_1 \in$(600 mV, 2.2 V), $v_3 \in$(−10 V, 10 V), c) generated chaotic waveform in time domain with final time 14 mS, and d) continuous frequency spectrum ending with component 10 kHz, logarithmic vertical range 10 μV up to 100 mV.

where $K = 0.1$ is internally trimmed transfer constant of analog multiplier. Note that electronic system (17) is equivalent

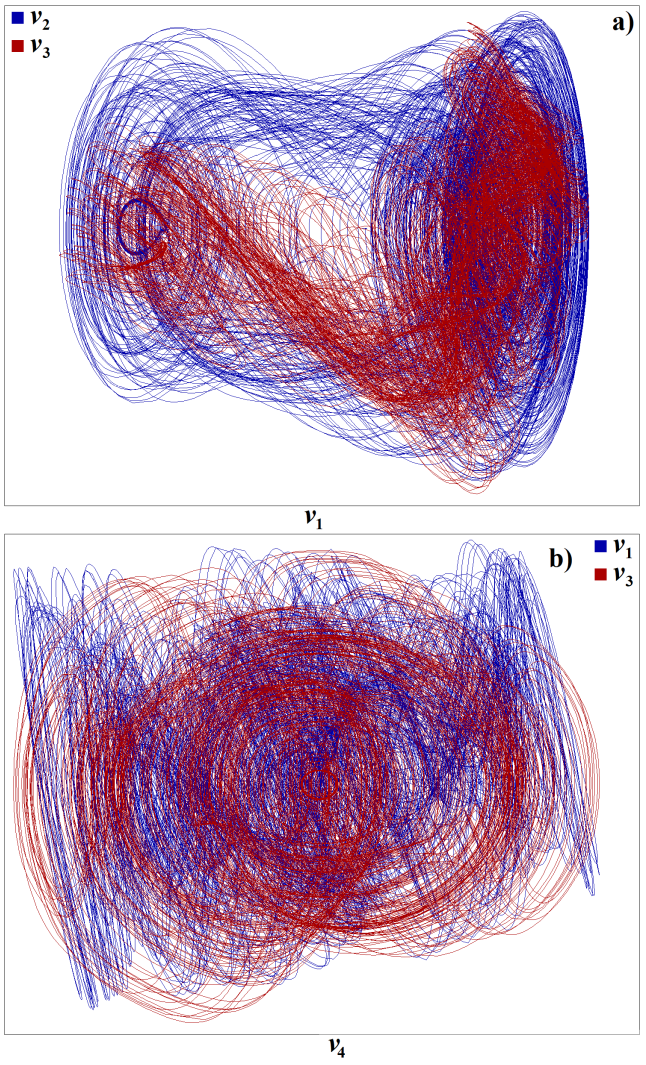

FIGURE 17. Orcad Pspice circuit simulation of dynamical system (18), ranges of individual state variables: a) horizontal axis $v_1 \in$(−2 V, 2.4 V), vertical scale $v_2 \in$(−2.5 V, 2 V), and $v_3 \in$(−6 V, 6 V), b) horizontal axis range $v_4 \in$(−7 V, 5 V), vertical axis scale is $v_1 \in$(−2.5 V, 2 V), $v_3 \in$(−6 V, 6 V).

to fiducial dynamical system (2) after introducing simple linear transformation of coordinates $v_1 \rightarrow -v_1$, $v_2 \rightarrow -v_2$, $v_3 \rightarrow -v_3$, and $i_L \rightarrow -v_4$. For time constant chosen for this oscillator $\tau = 1$ ms numerical values of the passive components are: $C = 100$ nF, $R_1 = 10$ kΩ, $R_2 = 10$ kΩ, $R_3 = 47$ Ω, $R_4 = 47$ kΩ, $R_5 = 2500$ Ω, $R_6 = 10$ kΩ, $R_7 = 2$ kΩ, and $R_8 = 47$ Ω.

Second chaotic circuit is visualized by means of Fig. 15. Behavior of this system is determined by the following set of the ordinary differential equations

$$\begin{aligned} \frac{d}{dt}v_1 &= -\frac{1}{R_4C}v_2,\ \frac{d}{dt}v_2 = -\frac{1}{R_7C}v_1 - \frac{1}{R_5C}v_2 - \frac{1}{R_2C}v_3 \\ &\quad + \frac{K^2}{R_3C}v_1^3,\ \frac{d}{dt}v_3 = -\frac{1}{R_6C}v_4 + \frac{K^2}{R_8C}v_2^3,\ \frac{d}{dt} \\ v_4 &= \frac{1}{R_1C}v_3, \end{aligned} \tag{18}$$

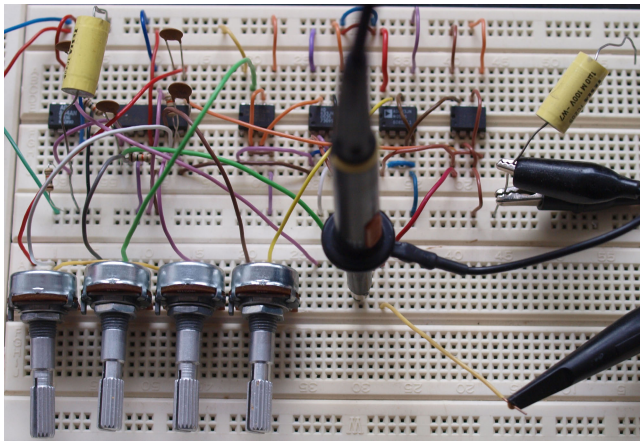

FIGURE 18. Breadboard with constructed chaotic oscillator, individual potentiometers represent coefficients of polynomial trans-conductance.

where $K = 0.1$ again. Note that transformation of coordinates $v_1 \rightarrow -v_1$, $v_2 \rightarrow -v_2$, $v_3 \rightarrow -v_3$, and $i_L \rightarrow -v_4$ has been adopted. Time constant chosen for this oscillator is $\tau = 1$ ms. Numerical values of passive components are: $C = 100$ nF, $R_1 = 10$ kΩ, $R_2 = 10$ kΩ, $R_3 = 47$ Ω, $R_4 = 47$ kΩ, $R_5 = 68$ kΩ, $R_6 = 10$ kΩ, $R_7 = 3300$ Ω, and $R_8 = 47$ Ω.

In both proposed circuitry realizations, the state variables are easily measurable as voltages at the outputs of inverting integrators. Supply voltage is symmetrical ±15 V and power dissipation is about 750 mW per supply branch. Six active devices are needed: single TL084 (four standard operational amplifiers within one package), current-feedback operational amplifier with external frequency compensation node AD844 (current-feedback amplifier) and four AD633 (four quadrant analog multipliers). Active elements mentioned above are chosen with respect to two factors: use only commercially available components and keep final chaotic oscillator cheap. On the other hand, frequency responses of mentioned active devices exhibit significant attenuation effects for the high frequency components of generated chaotic signals, i.e., band above 1 MHz. Interesting complete study about frequency limitations caused by the active elements in connection with design of the chaotic oscillators is provided in paper [56]. Authors focus on oscillators able to generate the multi-spiral attractors, that is problem of very precise circuit synthesis of vector field.

Full on-chip implementation of dynamical system (2) with arbitrary group of the internal parameters can be done easily. Particular technology for integration should be chosen with respect to state space volume occupied by prescribed strange attractor. Thus, especially following design factors require attention: supply voltage, voltage drops, current saturation levels and offset voltage. A very nice cookbook dealing with CMOS layout design of chaotic systems can be found in [29].

Because of a conventional integrator-block schematic that apply to a proposed chaotic oscillator it can be realized quite easily using FPAA development kits.

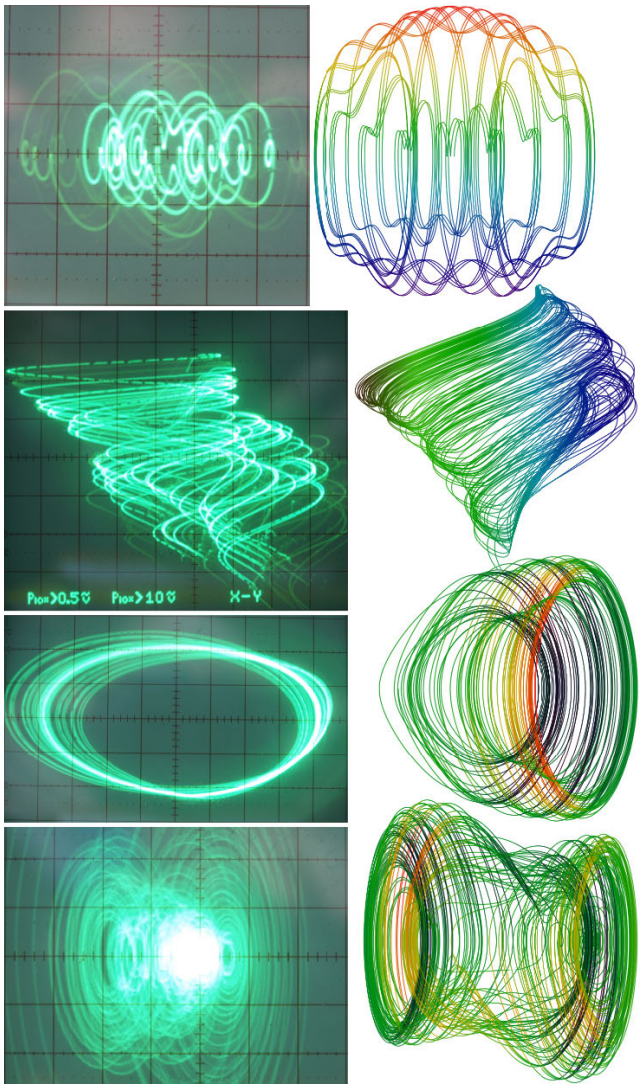

FIGURE 19. Experimental verification via oscilloscope screenshots: practical observation (left column) vs theoretical results (right column), different plane projections are used for this visualization.

VI. CIRCUIT SIMULATION AND MEASUREMENT

Both circuits given in Fig. 14 and Fig. 15 were implemented in Orcad Pspice simulation software. Simulation profile was set to final time 100 ms with the maximum allowed time step reduced to 10 μs. Few time domain results are provided by means of Fig. 16 and Fig. 17.

Photo of experimental setup implemented onto breadboard is illustrated by means of Fig. 18. True experimental outputs are provided within Fig. 19 where selected plane projections captured by analog-output oscilloscope are directly compared to theoretically equivalent trajectories numerically integrated using Mathcad environment. Laboratory experiments reveal strange attractors unobserved during numerical analysis and some of these are visualized in Fig. 20. Thus, concrete values of circuit parameters leading to these images are not given.

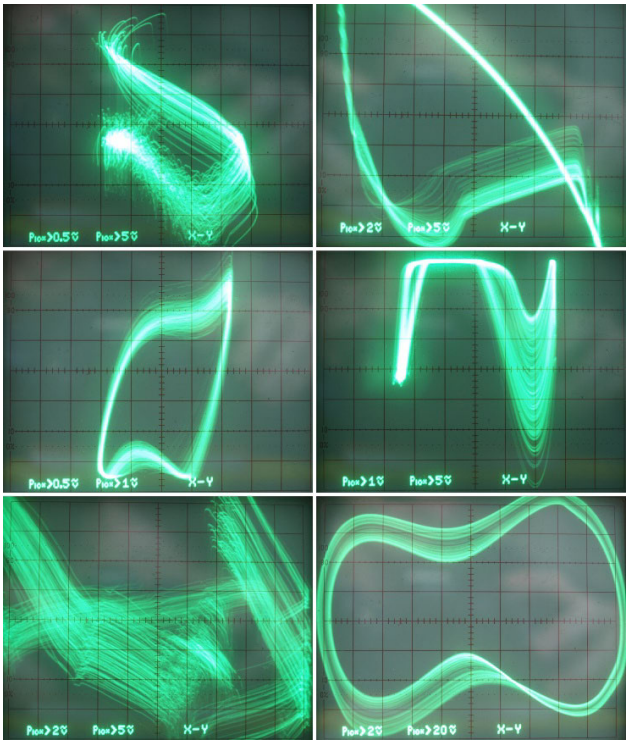

FIGURE 20. Experimental verification via oscilloscope screenshots: several plane projections of the selected chaotic attractors that were unnoticed during numerical investigation of dynamical system (2).

VII. CONCLUSION

During computer-aided numerical analysis of GBT-based cascaded class C amplifier a novel autonomous hyperchaotic dynamical system was discovered. Subsequent application of conventional flow quantification routines reveals two facts:

1. internal system parameters of the analyzed dynamical system can be calculated and/or adjusted such that generated hyperchaotic behavior is very robust, strongly unpredictable (with respect to the time scale),

2. mentioned hyperchaotic motion is easily modellable and experimentally measurable by the flow-equivalent electronic circuit, where only off-the-shelf components are used,

3. presence of GBT cells inside radiofrequency functional blocks causes almost ideal conditions for the evolution of the strange attractors. Smooth nonlinear saturation-type forward trans-conductance of each GBT causes both the vector field folding and stretching mechanism required for generation of complex, noise-like dynamics. Therefore, electronic systems based on bipolar transistors such as current mirrors, cascoded amplifiers, differential stages, negative resistance oscillator, and others clearly deserve to be addressed in near future and searching for chaos is highly recommended.

Personal experience of author with laboratory experiments confirms extreme sensitivity of a designed oscillator steady state to measurement setup (both initial conditions and values of the circuit components).

REFERENCES

[1] J. C. Sprott, "Some simple chaotic jerk functions," *Amer. J. Phys.*, vol. 65, no. 6, pp. 537–543, Jun. 1997, doi: 10.1119/1.18585.

[2] J. C. Sprott and S. J. Linz, "Algebraically simple chaotic flows," *Int. J. Chaos Theory Appl.*, vol. 5, no. 2, pp. 3–22, 2000.

[3] J. C. Sprott, "Simplest dissipative chaotic flow," *Phys. Lett. A*, vol. 228, nos. 4–5, pp. 271–274, 1997, doi: 10.1016/S0375-9601(97)00088-1.

[4] J. C. Sprott, "Some simple chaotic flows," *Phys. Rev. E, Stat. Phys. Plasmas Fluids Relat. Interdiscip. Top.*, vol. 50, no. 2, pp. 647–650, 1994, doi: 10.1103/PhysRevE.50.R647.

[5] B. Munmuangsaen, B. Srisuchinwong, and J. C. Sprott, "Generalization of the simplest autonomous chaotic system," *Phys. Lett. A*, vol. 375, no. 12, pp. 1445–1450, 2011, doi: 10.1016/j.physleta.2011.02.028.

[6] H. P. W. Gottlieb and J. C. Sprott, "Simplest driven conservative chaotic oscillator," *Phys. Lett. A*, vol. 291, no. 6, pp. 385–388, 2001, doi: 10.1016/S0375-9601(01)00765-4.

[7] T. Matsumoto, "A chaotic attractor from Chua's circuit," *IEEE Trans. Circuit Syst.*, vol. 31, no. 12, pp. 1055–1058, Dec. 1984, doi: 10.1109/TCS.1984.1085459.

[8] L. O. Chua and G. N. Lin, "Canonical realization of Chua's circuit family," *IEEE Trans. Circuit Syst.*, vol. 37, no. 7, pp. 885–902, Jul. 1990, doi: 10.1109/31.55064.

[9] M. Guzan, "Variations of boundary surface in Chua's circuit," *Radioengineering*, vol. 37, no. 7, pp. 885–902, 1990, doi: 10.1109/31.55064.

[10] S. C. Yener and H. H. Kuntman, "Fully CMOS memristor based chaotic circuit," *Radioengineering*, vol. 23, no. 4, pp. 1140–1149, 2014.

[11] S. Jafari, J. C. Sprott, V.-T. Pham, and S. M. R. H. Golpayegani, "A new cost function for parameter estimation of chaotic systems using return maps as fingerprints," *Int. J. Bifurcation Chaos*, vol. 24, no. 10, pp. 1567–1580, 2014, doi: 10.1142/S021812741450134X.

[12] J. Petrzela, "Optimal piecewise-linear approximation of quadratic chaotic dynamics," *Radioengineering*, vol. 21, no. 1, pp. 20–28, 2012.

[13] M. J. Ogorzalek, "Order and chaos in a third-order RC ladder network with nonlinear feedback," *IEEE Trans. Circuits Syst.*, vol. 36, no. 9, pp. 1221–1232, Sep. 1989, doi: 10.1109/31.34668.

[14] P. Bernat and I. Balaz, "RC autonomous circuits with chaotic behavior," *Radioengineering*, vol. 11, no. 2, pp. 1–5, 2002.

[15] A. S. Elwakil and M. P. Kennedy, "A semi-systematic procedure for producing chaos from sinusoidal oscillators using diode-inductor and FET-capacitor composites," *IEEE Trans. Circuits Syst. I, Fundam. Theory Appl.*, vol. 47, no. 4, pp. 582–590, Apr. 2000, doi: 10.1109/81.841862.

[16] A. S. Elwakil and M. P. Kennedy, "Chaotic oscillator configuration using a frequency dependent negative resistor," *J. Circuits, Syst. Comput.*, vol. 9, no. 3, pp. 229–242, 1999, doi: 10.1142/S0218126699000190.

[17] J. Petrzela and L. Polak, "Minimal realizations of autonomous chaotic oscillators based on trans-immittance filters," *IEEE Access*, vol. 7, pp. 17561–17577, 2019, doi: 10.1109/ACCESS.2019.2896656.

[18] R. Kiliç and F. Yildirim, "A survey of Wien bridge-based chaotic oscillators: Design and experimental issues," *Chaos, Solitons Fractals*, vol. 38, no. 5, pp. 1394–1410, 2008, doi: 10.1016/j.chaos.2008.02.016.

[19] O. Morgul, "Wien bridge based RC chaos generator," *Electron. Lett.*, vol. 31, no. 24, pp. 2058–2059, Nov. 1995, doi: 10.1049/el:19951411.

[20] K. Rajagopal, C. Li, F. Nazarimehr, A. Karthikeyan, P. Duraisamy, and S. Jafari, "Chaotic dynamics of modified Wien bridge oscillator with fractional order memristor," *Radioengineering*, vol. 28, no. 1, pp. 165–174, 2019, doi: 10.13164/re.2019.0165.

[21] M. P. Kennedy, "Chaos in the Colpitts oscillator," *IEEE Trans. Circuits Syst. I, Fundam. Theory Appl.*, vol. 41, no. 11, pp. 771–774, Nov. 1994, doi: 10.1109/81.331536.

[22] P. Kvarda, "Chaos in Hartley's oscillator," *Int. J. Bifurcation Chaos*, vol. 12, no. 10, pp. 2229–2232, 2002, doi: 10.1142/S0218127402005777.

[23] M. Itoh, "Synthesis of electronic circuits for simulating nonlinear dynamics," *Int. J. Bifurcation Chaos*, vol. 11, no. 3, pp. 605–653, 2001, doi: 10.1142/S0218127401002341.

[24] J. Petržela, Z. Hruboš, and T. Gotthans, "Modeling deterministic chaos using electronic circuits," *Radioengineering*, vol. 20, no. 2, pp. 438–444, 2011.

[25] V. T. Pham, D. S. Ali, N. M. G. Al-Saidi, K. Rajagopal, F. E. Alsaadi, and S. Jafari, "A novel mega-stable chaotic circuit," *Radioengineering*, vol. 29, no. 1, pp. 140–146, 2020, doi: 10.13164/re.2020.0140.

[26] R. Trejo-Guerra, E. Tlelo-Cuautle, V. H. Cabajal-Gómez, and G. Rodriguez-Gómez, "A survey on the integrated design of chaotic oscillators," *Appl. Math. Comput.*, vol. 219, no. 10, pp. 5113–5122, 2013, doi: 10.1016/j.amc.2012.11.021.

[27] T. Götthans and J. Petržela, "Experimental study of the sampled labyrinth chaos," *Radioengineering*, vol. 20, no. 4, pp. 873–879, 2011.

[28] J. Petržela, T. Gotthans, and M. Guzan, "Current-mode network structures dedicated for simulation of dynamical systems with plane continuum of equilibrium," *J. Circuits, Syst. Comput.*, vol. 27, no. 9, 2018, Art. no. 1830004, doi: 10.1142/S0218126618300040.
[29] V. H. Carbajal-Gomez, E. Tlelo-Cuautle, J. M. Munoz-Pacheco, L. G. D. L. Fraga, C. Sanchez-Lopez, and F. V. Fernandez-Fernandez, "Optimization and CMOS design of chaotic oscillators robust to PVT variations," *Integration*, vol. 65, pp. 32–42, 2019, doi: 10.1016/j.vlsi.2018.10.010.
[30] A. Silva-Juarez, E. Tlelo-Cuautle, L. G. D. L. Fraga, and R. Li, "FPAA-based implementation of fractional-order chaotic oscillators using first-order active filter blocks," *J. Adv. Res.*, vol. 25, pp. 77–85, Sep. 2020, doi: 10.1016/j.jare.2020.05.014.
[31] E. Tlelo-Cuautle, A. D. Pano-Azucena, O. Guillen-Fernandez, and A. Silva-Juarez, *Analog/Digital implementation of Fractional Order Chaotic Circuits and Applications*. Springer, 2020, pp. 41–74.
[32] K. Rajagopal, S. T. Kingni, A. J. M. Khalaf, Y. Shekofteh, and F. Nazarimehr, "Coexistence of attractors in a simple chaotic oscillator with fractional-order-memristor component: Analysis, FPGA implementation, chaos control and synchronization," *Eur. Phys. J. Special Topics*, vol. 228, pp. 2035–2051, Oct. 2019, doi: 10.1140/epjst/e2019-900001-8.
[33] K. Rajagopal, A. Akgul, A. Karthikeyan, I. Koyuncu, and S. Jafari, "Chaotic chameleon: Dynamic analyses, circuit implementation, FPGA design and fractional-order form with basic analyses," *Chaos, Solitons Fractals*, vol. 103, pp. 476–487, Oct. 2017, doi: 10.1016/j.chaos.2017.07.007.
[34] A. Sambas, S. Vaidyanathan, E. Tlelo-Cuautle, B. Abd-El-Atty, A. A. A. El-Latif, O. Guille-Fernandez, Sukono, Y. Hidayat, and G. Gundara, "A 3-D multi-stable system with a peanut-shaped equilibrium curve: Circuit design, FPGA realization, and an application to image encryption," *IEEE Access*, vol. 8, pp. 137116–137132, 2020. [Online]. Available: https://ieeexplore.ieee.org/document/9146866/authors
[35] A. Sambas, S. Vaidyanathan, E. Tlelo-Cuautle, S. Zhang, O. Guillen-Fernandez, Y. Hidayat, and G. Gundara, "A novel chaotic system with two circles of equilibrium points: Multistability, electronic circuit and FPGA realization," *Electronics*, vol. 8, no. 11, p. 1211, Oct. 2019, doi: 10.3390/electronics8111211
[36] O. Guillen-Fernandez, M. F. Moreno-Lopez, and E. Tlelo-Cuautle, "Issues on applying one- and multi-step numerical methods to chaotic oscillators for FPGA implementation," *Mathematics*, vol. 9, no. 2, p. 151, 2021, doi: 10.3390/math9020151.
[37] J. Petržela, "On the existence of chaos in the electronically adjustable structures of the state variable filters," *Int. J. Circuit Theory Appl.*, vol. 44, no. 10, pp. 1779–1797, 2016, doi: 10.1002/cta.2193.
[38] H. H. C. Lu, D. S. Yu, A. L. Fitch, V. Sreeram, and H. Chen, "Controlling chaos in a memristor based circuit using a twin-T notch filter," *IEEE Trans. Circuits Syst. I, Reg. Papers*, vol. 58, no. 6, pp. 1337–1344, Jun. 2011, doi: 10.1109/TCSI.2010.2097771.
[39] J. H. B. Deane, "Chaos in a current-mode controlled boost DC-DC converter," *IEEE Trans. Circuits Syst. I, Fundam. Theory Appl.*, vol. 39, no. 8, pp. 680–683, Aug. 1992, doi: 10.1109/81.168922.
[40] E. Fossas and G. Olivar, "Study of chaos in the buck converter," *IEEE Trans. Circuits Syst. I, Fundam. Theory Appl.*, vol. 43, no. 1, pp. 13–25, Jan. 1996, doi: 10.1109/81.481457.
[41] D. C. Hamill and D. J. Jeffries, "Subharmonics and chaos in a controlled switched-mode power converter," *IEEE Trans. Circuits Syst.*, vol. 35, no. 8, pp. 1059–1061, Aug. 1988, doi: 10.1109/31.1858.
[42] C. K. Tse, "Flip bifurcation and chaos in three-state boost switching regulators," *IEEE Trans. Circuits Syst. I, Fundam. Theory Appl.*, vol. 41, no. 1, pp. 16–23, Jan. 1994, doi: 10.1109/TCS.1985.1085626.
[43] A. Rodriguez-Vazquez, J. Huertas, and L. Chua, "Chaos in switched-capacitor circuit," *IEEE Trans. Circuits Syst.*, vol. CS-32, no. 10, pp. 1083–1085, Oct. 1985, doi: 10.1109/TCS.1985.1085626.
[44] J. Petrzela, "Multi-valued static memory with resonant tunneling diodes as natural source of chaos," *Nonlinear Dyn.*, vol. 94, pp. 1867–1887, Jul. 2018, doi: 10.1007/s11071-018-4462-0.
[45] T. Endo and L. O. Chua, "Chaos from phase-locked loops," *IEEE Trans. Circuits Syst.*, vol. 35, no. 8, pp. 987–1003, Aug. 1988, doi: 10.1109/31.1845.
[46] T. Endo, "A review of chaos and nonlinear dynamics in phase-locked loops," *J. Franklin Inst.*, vol. 331, no. 6, pp. 859–902, 1994, doi: 10.1016/0016-0032(94)90091-4.
[47] J. Petrzela, "Generalized single stage class C amplifier: Analysis from the viewpoint of chaotic behavior," *Appl. Sci.*, vol. 10, no. 15, p. 5025, 2020, doi: 10.3390/app10155025.
[48] J. Petrzela, "Evidence of strange attractors in class C amplifier with single bipolar transistor: Polynomial and piecewise-linear case," *Entropy*, vol. 23, no. 2, p. 175, 2021, doi: 10.3390/e23020175.
[49] J. Petrzela, "New chaotic oscillator derived from class C single transistor-based amplifier," *Math. Problems Eng.*, vol. 2020, Nov. 2020, Art. no. 2640629, doi: 10.1155/2020/2640629.
[50] A. Silva-Juarez, E. Tlelo-Cuautle, L. G. D. L. Fraga, and R. Li, "Optimization of the Kaplan-Yorke dimension in fractional-order chaotic oscillators by metaheuristics," *Appl. Math. Comput.*, vol. 394, Apr. 2021, Art. no. 125831, doi: 10.1016/j.amc.2020.125831.
[51] J. C. Sprott, *Chaos and Time Series Analysis*. Oxford, U.K.: Oxford Univ. Press, 2003, pp. 104–126.
[52] K. Grygiel and P. Szlachetka, "Lyapunov exponent analysis of autonomous and nonautonomous set of ordinary differential equations," *Acta Phys. Polonica B*, vol. 26, no. 8, pp. 1321–1331, 1995.
[53] P. Frederickson, J. L. Kaplan, E. D. Yorke, and J. A. Yorke, "The Liapunov dimension of strange attractors," *J. Differ. Equ.*, vol. 49, no. 2, pp. 185–207, 1983, doi: 10.1016/0022-0396(83)90011-6.
[54] S. Jafari, J. C. Sprott, and F. Nazarimehr, "Recent new examples of hidden attractors," *Eur. Phys. J. Special Topics*, vol. 224, pp. 1469–1476, Jul. 2015, doi: 10.1140/epjst/e2015-02472-1.
[55] G. A. Leonov and N. V. Kuznetsov, "Hidden attractors in dynamical systems. Form hidden oscillations in Hilbert-Kolmogorov, Aizerman, and Kalman problems to hidden chaotic attractors in Chua circuit," *Int. J. Bifurcation Chaos*, vol. 23, no. 1, 2013, Art. no. 1330002, doi: 10.1142/S0218127413300024.
[56] J. M. Munoz-Pacheco, E. Tlelo-Cuautle, I. Toxqui-Toxqui, C. Sanchez-Lopez, and R. Trejo-Guerra, "Frequency limitations in generating multi-scroll chaotic attractors using CFOAs," *Int. J. Electron.*, vol. 101, no. 11, pp. 1559–1569, 2014, doi: 10.1080/00207217.2014.880999.

JIRI PETRZELA was born in Brno, Czech Republic, in 1978. He received the M.Sc. and Ph.D. degrees in theoretical electronics in 2003 and 2007, respectively. He is currently working as an Associate Professor with the Department of Radio Electronics, Faculty of Electrical Engineering and Communications, Brno University of Technology, Czech Republic. He is the main author of more than 20 journal articles and 30 international conference contributions. His research interests include nonlinear dynamics, chaos theory, numerical methods, analog lumped circuit design, and computer-aided analysis.